Nanoelectronics and Its New Materials – A NEW ERA OF NANOSCIENCE

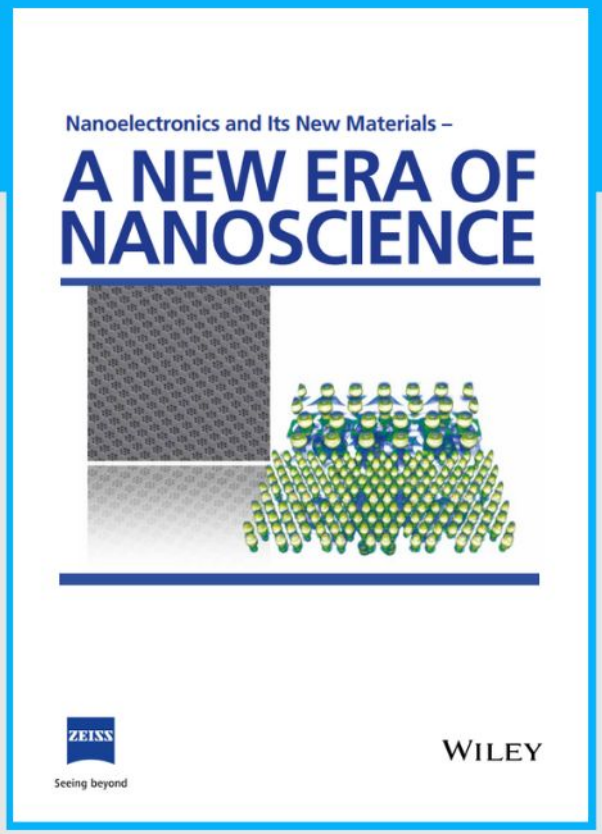

Discover the recent advances in electronics research and fundamental nanoscience.

Nanotechnology has become the driving force behind breakthroughs in engineering, materials science, physics, chemistry, and biological sciences. In this compendium, we delve into a wide range of novel applications that highlight recent advances in electronics research and fundamental nanoscience. From surface analysis and defect detection to tailored optical functionality and transparent nanowire electrodes, this eBook covers key topics that will revolutionize the future of electronics.

To get your hands on this valuable resource and unleash the power of nanotechnology, simply download the eBook now. Stay ahead of the curve and embrace the future of electronics with nanoscience as your guide.

ZEISS

Seeing beyond

WILEY

ADVANCED FUNCTIONAL MATERIALS
www.afm-journal.de

Efficient and Thermally Stable Wide Bandgap Perovskite Solar Cells by Dual-Source Vacuum Deposition

Lidón Gil-Escrig, Isidora Susic, İlker Doğan, Valerio Zardetto, Mehrdad Najafi, Dong Zhang, Sjoerd Veenstra, Salar Sedani, Bulent Arikan, Selcuk Yerci, Henk J. Bolink, and Michele Sessolo**

Wide bandgap perovskites are being widely studied in view of their potential applications in tandem devices and other semitransparent photovoltaics. Vacuum deposition of perovskite thin films is advantageous as it allows the fabrication of multilayer devices, fine control over thickness and purity, and it can be upscaled to meet production needs. However, the vacuum processing of multicomponent perovskites (typically used to achieve wide bandgaps) is not straightforward, because one needs to simultaneously control several thermal sources during the deposition. Here a simplified dual-source vacuum deposition method to obtain wide bandgap perovskite films is shown. The solar cells obtained with these materials have similar or even larger efficiency as those including multiple A-cations, but are much more thermally stable, up to 3500 h at 85 °C for a perovskite with a bandgap of 1.64 eV. With optimized thickness, record efficiency of >19% and semitransparent devices with stabilized power output in excess of 17% are achieved.

1. Introduction

Organic–inorganic (hybrid) metal halide perovskites are direct bandgap semiconductors with potential applications in several optoelectronic devices. They have extensively been investigated in thin film solar cells, reaching record efficiency for single junction devices based on lead perovskites exceeding 25.5%.[1,2] One important feature of this family of compounds is the possibility to fine tune the energy bandgap (E_g) from the near infrared (NIR) to the UV part of the electromagnetic spectrum. The most efficient solar cells are obtained with formamidinium lead iodide ($FAPbI_3$, or FAPI), with E_g = ≈1.5 eV. By partial substitution of Pb^{2+} with Sn^{2+}, the bandgap can be lowered to ≈1.2 eV,[3,4] while partial substitution of iodide with a more electronegative halide (bromide and chloride), allows to tune E_g up to and beyond 3 eV.[5,6] These characteristics allow the preparation of tandem devices,[7] with the potential to overcome the efficiency limit of single junction solar cells. Several device architectures are being developed, in particular perovskite/perovskite tandems,[8–14] tandems of perovskite with CIGS[15,16] or even with organic semiconductors,[17] and perovskite/silicon devices, which can be built in a 4-terminal (4T) configuration,[18–24] as well as in a monolithic 2-terminal (2T) structure.[25–30] The latter is particularly promising, as PCEs approaching 30% have been demonstrated.[28,30] To maximize the efficiency of tandem solar cells, wide bandgap perovskites with E_g ranging from 1.68 eV (for perovskite/silicon) to 1.80 eV (for perovskite/perovskite) should be employed.[31] Wide bandgap perovskites can be obtained with mixed iodide/bromide compositions, where also mixed A-site cations (FA^+, Cs^+) are typically employed to improve the photo- and thermal stability of the compounds.[32–40] The majority of reports on perovskite solar cells are based on solution-processing techniques. Vacuum processing is being increasingly investigated, in view of its potential for upscaling,[41,42] fine control of the film thickness,[43,44] and easier fabrication of multilayer devices.[45] The efficiency of solar cells with co-evaporated perovskites has reached significant PCE (≈20%),[46–48] but has long lagged behind that of solution-processed devices. A recent report of sequential vacuum deposited perovskite films demonstrated PCE in excess of 24%, narrowing the gap with solution-processed solar cells.[49]

Only a few reports of wide bandgap perovskite solar cells fabricated by vacuum deposition exist. Mixed iodide/bromide

L. Gil-Escrig, I. Susic, H. J. Bolink, M. Sessolo
Instituto de Ciencia Molecular
Universidad de Valencia
46980 Paterna, Spain
E-mail: lidon.gil@uv.es; michele.sessolo@uv.es
İ. Doğan, V. Zardetto, M. Najafi, D. Zhang, S. Veenstra
TNO – Solliance
5656AE Eindhoven, The Netherlands
S. Sedani, B. Arikan, S. Yerci
ODTÜ GÜNAM
Middle East Technical University
Ankara 06800, Turkey
S. Yerci
Department of Electrical-Electronics Engineering and
Department of Micro and Nanotechnology
Middle East Technical University
Ankara 06800, Turkey
The ORCID identification number(s) for the author(s) of this article can be found under https://doi.org/10.1002/adfm.202214357.

DOI: 10.1002/adfm.202214357

formulations with double and triple A-site cations have been reported.[50–53] However, in most cases they are found to be thermally unstable when stressed at 85 °C unless complex compositions involving four A-site cations are used.[53] Interestingly, and in apparent contradiction with what is observed for perovskites processed from solution,[54] vacuum-deposited pure methylammonium (MA^+) perovskites are much more stable than those based on multi-cation formulations. Methylammonium lead iodide ($MAPbI_3$, or MAPI) deposited by co-evaporation has been found stable for thousands of hours when continuously stressed at 85 °C.[55,56] Pure MA-based wide bandgap perovskites, obtained by co-evaporation of MAI, PbI_2 and $PbBr_2$ have also been reported,[57,58] along with materials obtained via sequential hybrid processes,[59] however, their thermal stability has not yet been assessed. In this work, we report a simplified process for the preparation of pure MA-based perovskite films by the simultaneous sublimation of MAI and a pre-synthesized mixed halide lead precursor. By changing the I/Br content in the $Pb(I_{1-n}Br_n)_2$ precursor, the bandgap of the $MAPb(I_{1-x}Br_x)_3$ wide bandgap perovskites can be readily tuned. Vacuum deposited solar cells obtained with these materials have similar or even larger PCEs as those including multiple A-cations, but are much more thermally stable, up to 3500 h at 85 °C for a perovskite with a bandgap of 1.64 eV. With optimized thickness, we achieved record PCE > 19% for a bandgap of 1.64 eV. We applied these wide bandgap perovskites in semitransparent (ST) device configurations, reaching stabilized power output in excess of 17%. Note that the concept of semitransparency as used in our manuscript, refers to devices that are bifacial, that is, where both electrodes are transparent. The devices have actually very low transparency in the visible part of the electromagnetic spectrum, as the thick perovskite films absorb most of the above-bandgap photons. Proof-of-concept 4T-tandem devices using ST perovskite cells in combination with mainstream silicon solar cells are also presented.

2. Results and Discussion

In order to simplify the deposition of $MAPb(I_{1-x}Br_x)_3$ to a dual-source process, we prepared a mixed halide $Pb(I_{1-n}Br_n)_2$ precursor by adding PbI_2 and $PbBr_2$ in stoichiometric amounts in a crucible and melting them at 350 °C in nitrogen at atmospheric pressure. In this way, we obtained a mixture which sublimes without substantial changes in its stoichiometry during the duration of the typical deposition process (Figures S1–S3, Supporting Information). The mixture is homogeneous in appearance and contains a mixed $Pb(I_{1-x}Br_x)_2$ phase, although not quantitatively as the precursors are still present after melting.[60] Similar approaches have been previously used by us and others to reduce the number of deposition sources in the vacuum processing of multi-cation/halide perovskites.[53,61] $MAPb(I_{1-x}Br_x)_3$ perovskite films were prepared by dual source deposition starting from MAI and mixtures of increasing bromide/iodide ratios (Figure S4, Supporting Information), specifically $Pb(I_{0.9}Br_{0.1})_2$, $Pb(I_{0.8}Br_{0.2})_2$, and $Pb(I_{0.7}Br_{0.3})_2$. Previous works highlighted the difficulties associated with the sublimation control of MAI,[62,63] hence we have adopted a recently reported protocol based on a two source/two sensors system, which ensures a reliable and reproducible deposition process.[64,65] The corresponding Tauc plots obtained from the absorption spectra (**Figure 1**a) show the expected blue-shift of the absorption cutoff when increasing the bromide contents, leading to wider bandgap perovskites with bandgaps (E_g) of 1.64, 1.68, and 1.71 eV. Photoluminescence (PL) spectra (Figure 1b) also shows the shift of the bandgap with increasing bromide content. The PL peaks for perovskites obtained from $Pb(I_{0.9}Br_{0.1})_2$, $Pb(I_{0.8}Br_{0.2})_2$, and $Pb(I_{0.7}Br_{0.3})_2$ precursors are centered at 755, 740, and 724 nm, respectively, in agreement with the optical bandgap estimated via the Tauc plot (1.64, 1.68 and 1.71 eV). The PL spectra obtained upon excitation with a 515 nm laser at carrier concentration equal to 1 sun illumination consist of a single signal with no detectable low-energy component, suggesting that halide segregation is absent in as-prepared films. Even longer measurements (30 min) under continuous laser illumination do not show the appearance of low energy features (Figure S5, Supporting Information).

The relative halide concentrations in the perovskite samples were estimated by energy dispersive X-ray (EDS) spectroscopy. From the bromide/iodide ratio we calculated the bromide fraction x in the chemical formula $MAPb(I_{1-x}Br_x)_3$, and compare it with the initial bromide content n in the mixed halide precursor $Pb(I_{1-n}Br_n)_2$ (Figure 1c). We observed a systematic reduction of the amount of bromide during the conversion to perovskite, which is expected as the lead halide precursor reacts with MAI. The final Br content is 70%–80% of the initial values, leading to perovskite with nominal compositions of $MAPb(I_{0.92}Br_{0.08})_3$, $MAPb(I_{0.86}Br_{0.14})_3$, and $MAPb(I_{0.79}Br_{0.21})_3$, corresponding to optical bandgaps of 1.64, 1.68, and 1.71 eV, respectively. The X-ray diffraction (XRD) of the three materials shows similar patterns (Figure 1d), compatible with a cubic perovskite, with an intense signal at $2\theta = 14.05°$, corresponding to the (002) perovskite plane.[56] Conversion to the perovskite phase seems quantitative in all cases, as only the perovskite films with 1.68 eV bandgap show a minor contribution of residual PbI_2, denoted by the reflection at $2\theta = 12.5°$. The origin of this weak but appreciable signal is not clear yet, but it seems to not be detrimental to the device functioning, as also observed previously for pure $MAPbI_3$.[56] The surface morphology of the $MAPb(I_{1-x}Br_x)_3$ films were imaged with scanning electron microscopy (SEM, Figure S6, Supporting Information). The lowest bandgap perovskite films show a compact morphology, with randomly oriented grains with a size in the 100–200 nm range. When more bromide is added to the material, the grain size is slightly reduced and the morphology appears more disordered, with other small features formed on the perovskite surface. In general, the materials are very compact with no voids, as commonly observed for vacuum deposited perovskites.[46,47,66]

The perovskite films were tested in fully vacuum-processed solar cells in the p-i-n configuration. Devices were built on indium tin oxide (ITO) patterned glass substrates, and a thin (3 nm) layer 2,2“,7,7”-Tetra(N,N-di-p-tolyl)amino-9,9-spirobifluorene (Spiro-TTB) was used as the hole transport layer (HTL), as it can be used as a standalone material without any high work function interlayers at the ITO/HTL interface.[67,68] A 450 nm thick wide bandgap perovskite was evaporated onto the Spiro-TTB, and coated with carbon 60 fullerene (C_{60}, 25 nm) and bathocuproine BCP (8 nm) as electron transport layers

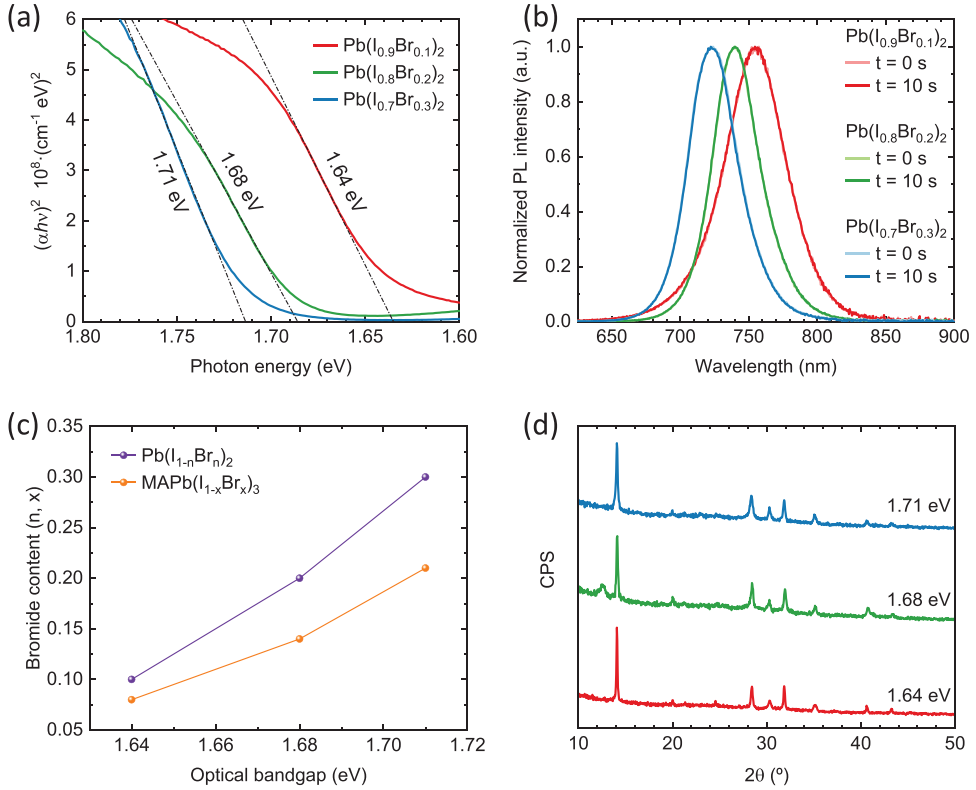

Figure 1. a) Tauc plot calculated from optical absorption for three different mixed halide precursors with increasing bromide content. b) Photoluminescence spectra of the perovskite samples on ITO/glass substrates under laser excitation at 515 nm (1 sun equivalent intensity), at time 0 and after 10 s of continuous illumination. c) Bromide content in the perovskite (*x*) was estimated by EDS and compared with the bromide content in the mixed halide precursor (*n*). d) XRD patterns for the three different perovskite films.

(ETLs). The thickness of the perovskite film was chosen to ensure sufficient current collection, although, with alternative vacuum-deposition methods, much thinner films with similar current collection efficiency have been reported.[69] The devices were finished with a 100 nm thick silver electrode. The solar cells were encapsulated with a 20 nm thick Al_2O_3 film deposited by a low temperature atomic layer deposition (ALD) process.[56]

As-prepared solar cells were characterized by measuring their current density versus voltage (*J-V*) curves under simulated solar illumination (**Figure 2**a). The corresponding photovoltaic parameters, PCE, fill factor (FF), open-circuit voltage (V_{oc}) and short circuit current density (J_{sc}) are reported in Figure 2c–f and in **Table 1**. For solar cells with varying perovskite bandgaps, we observed the expected trend of the V_{oc} and J_{sc}, that is, the photovoltage increases with the bandgap while the photocurrent decreases. The J_{sc} decreases monotonically from 18.5 to 15.0 mA cm^{-2} when the bandgap is increased from 1.64 to 1.71 eV. The V_{oc} was found to be 1.13 V for the 1.64 eV bandgap, and larger ≈1.17 V for the perovskite with 1.68 and 1.71 eV bandgap. The FF was found to be moderate, increasing from ≈65% to 70% with increasing perovskite bandgap. Overall, we obtained PCE of ≈13.5% and 14.0% for E_g of 1.64 and 1.68 eV, respectively, and of ≈12.5% for the wider bandgap material (1.71 eV). As the aim of this work was to assess the thermal stability of MAI-based vacuum deposited wide bandgap perovskites, we stressed the devices at 85 °C on a hot plate in ambient light and measured their performance periodically. The *J–V* curves under illumination and the corresponding parameters measured after 1 h at 85 °C are reported in Figure 2b,c–f, respectively. In general, we found a substantial improvement of the device performance, which is mainly driven by a better rectification, as the FF increases to 76%, 77%, and 74%, on average, for perovskite solar cells with bandgaps of 1.64, 1.68, and 1.71 eV, respectively. We also observed an increase in the V_{oc} for the 1.64 and 1.71 eV bandgap materials, up to 1.16 and 1.21 V, respectively. For all bandgaps, the photocurrent was also found to increase by 1–2 mA cm^{-2}. As a consequence, PCEs for the solar cells with 1.64, 1.68, and 1.71 eV bandgaps were found to reach average values of 17.7%, 16.7%, and 15.1%, respectively, after 1 h thermal stressing at 85 °C. The origin of the efficiency improvement is not clear yet. In a control experiment we performed annealing of the sample immediately after co-sublimation of the perovskite, and found no improvement in the device performance (Figure S7, Supporting Information). This indicates that most likely the performance enhancement is related with interface effects at the perovskite/ETL and/or ETL/Ag interface.

In order to assess the quality of the wide-bandgap $MAPb(I_{1-x}Br_x)_3$ perovskites and the corresponding solar cells, we investigated their EQE response in the bandgap region. From the semi-logarithmic plot in **Figure 3**a one can see for all devices a steep drop of the EQE around the perovskite's bandgap. From the linear slope of the EQE, we extracted the Urbach energies (E_U), which are in the 16–18 meV range,

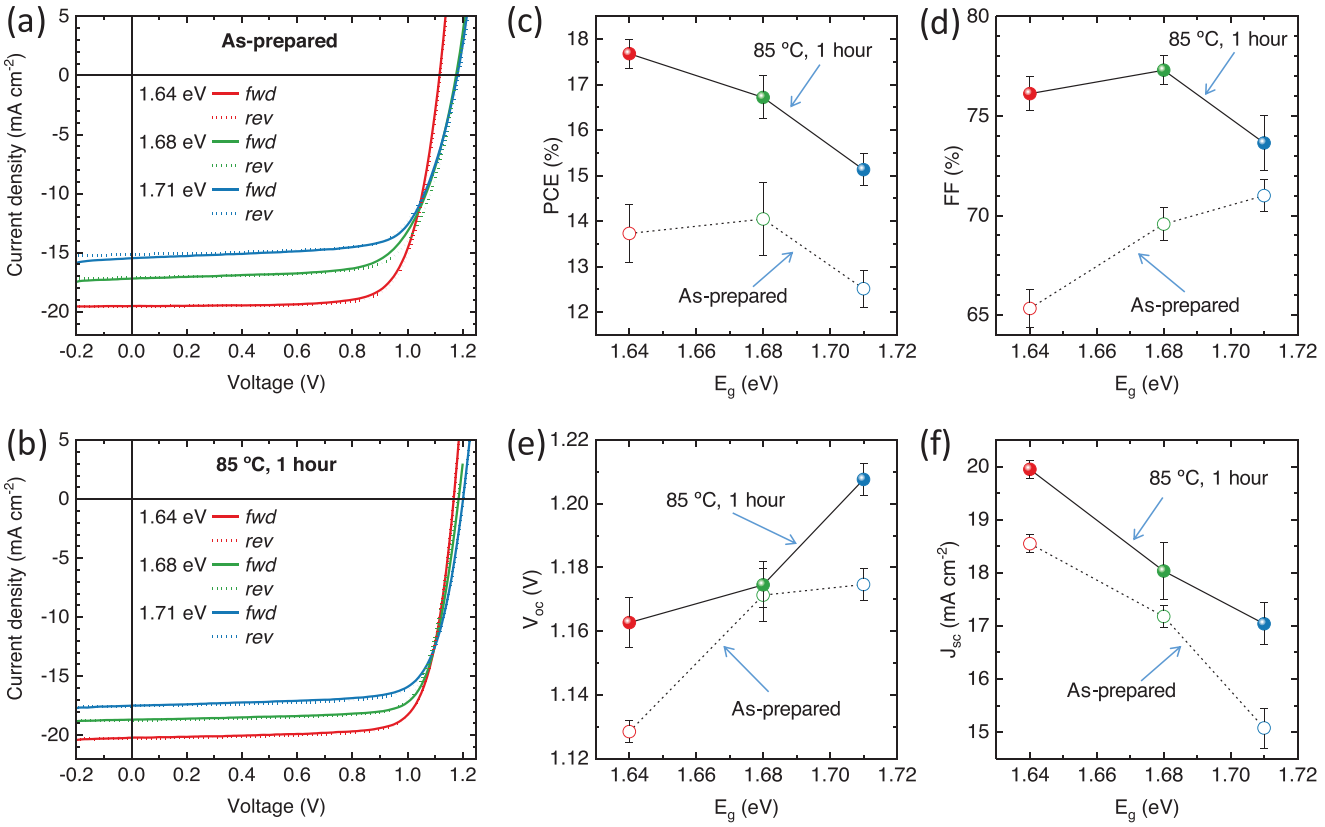

Figure 2. *J–V* curves measured under simulated solar illumination for solar cells with perovskites of increasing bandgap, collected for a) as-prepared devices and for b) devices stressed at 85 °C for 1 h in ambient light. c–f) Photovoltaic parameters as a function of the perovskite bandgap, for as-prepared (empty symbols, dashed lines) and thermally stressed (full symbols, solid lines) solar cells (lines are guides to the eye). The device layout is ITO/ Spiro-TTB (3 nm)/$MAPb(I_{1-x}Br_x)_3$ (450 nm)/C_{60} (25 nm)/BCP (8 nm)/Ag.

similar to previously reported mixed cation/mixed halide vacuum deposited wide bandgap perovskites.[52] The bandgaps estimated from the derivative of the EQE spectra (Figure S8, Supporting Information) agree well with those estimated with Tauc plots in Figure 1a (within a maximum deviation of 10 meV). In order to compare the limitations of solar cells based on perovskites with different bandgaps with each other, we calculated the ratio between the measured performance indicators as obtained from the *J–V* curves and their maximal obtainable values in the radiative limit (Figure 3b). The radiative limit of the V_{oc} was calculated via the EQE response,[70] while the FF and J_{sc} were obtained from detailed balance calculations for the specific material bandgap.[71] The V_{oc} loss was found to be rather independent of the bandgap, at 84%–86% of the theoretical maximum. One can notice a larger FF loss (80%) for the wider bandgap material, and a clear increase of the photocurrent losses when increasing the bandgap, as the J_{sc} decreases from 83% to 76% of the radiative limit. This results in larger PCE losses for the wider bandgap perovskite solar cells, standing at 52% of the maximum achievable PCE. For the lowest bandgap, the PCE is at ≈60% of its corresponding theoretical maximum. These differences might originate from variations in the charge diffusion length when increasing the bromide content in the $MAPb(I_{1-x}Br_x)_3$ perovskite.

In addition, we measured the absolute intensity PL spectra of the three $MAPb(I_{1-x}Br_x)_3$ perovskites film deposited on

Table 1. Average PV parameters for $MAPb(I_{1-x}Br_x)_3$ solar cells of increasing bandgap, measured for as-prepared devices and after thermal stressing for 1 h at 85 °C.

E_g [eV]		J_{sc} [mA cm^{-2}]	FF [%]	V_{oc} [V]	PCE [%]
1.64	As-prep.	18.55 ± 0.17	65 ± 1	1.13 ± 0.01	13.7 ± 0.6
	1 h 85°C	19.95 ± 0.17	76 ± 1	1.16 ± 0.01	17.7 ± 0.3
1.68	As-prep.	17.17 ± 0.21	70 ± 1	1.17 ± 0.01	14.1 ± 0.8
	1 h 85°C	18.03 ± 0.54	77 ± 1	1.17 ± 0.01	16.7 ± 0.5
1.71	As-prep.	15.08 ± 0.38	71 ± 1	1.17 ± 0.01	12.5 ± 0.4
	1 h 85°C	17.04 ± 0.40	74 ± 1	1.21 ± 0.01	15.1 ± 0.4

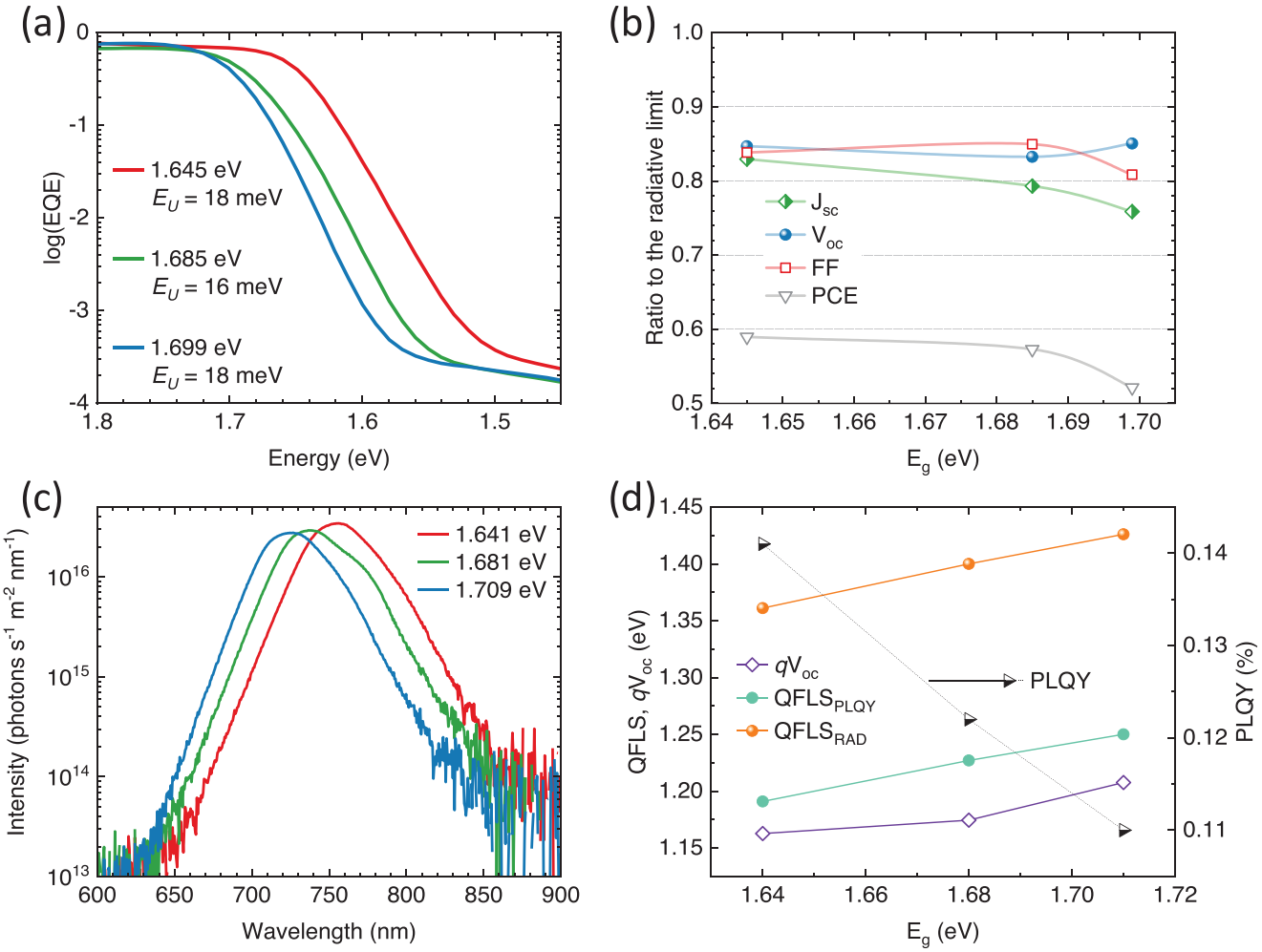

Figure 3. a) EQE spectra in the bandgap region and calculated bandgap and Urbach energies. b) The ratio of measured V_{oc}, J_{sc}, and FF to their maximum theoretical (radiative) limit (lines are guides to the eye). c) Absolute calibrated PL spectra of perovskite films on glass under laser excitation at 515 nm and 1 sun equivalent light intensity. d) Comparison of the measured qV_{oc}, QFLS calculated from PLQY ($QFLS_{PLQY}$) and QFLS in the radiative limit ($QFLS_{RAD}$) as a function of the perovskite bandgap, which is estimated from a bi-Gaussian fit of the PL spectrum. Analysis is based on devices stressed at 85 °C for 1 h.

glass (Figure 3c). The PL peak centers were calculated via a bi-Gaussian fit of the spectra, which corresponds to the optical bandgap of the perovskites. The PL spectrum of the perovskite with 1.68 eV bandgap shows a low energy component which is, however, not associated with halide segregation but rather originates from photon reabsorption and cavity effects.[44,72] This is also supported by the fact that the PL of the same samples deposited on ITO do not show the low energy component (Figure 1b), and that it is absent for the perovskite with the wider bandgap, where more bromide is inserted. We calculated the PL quantum yield (PLQY) and the corresponding quasi-Fermi level splitting ($QFLS_{PLQY}$), which sets the upper limit for the attainable V_{oc}. In Figure 3d, these parameters are compared to the QFLS in the radiative limit ($QFLS_{RAD}$). The PLQY for the bare perovskite films was found to be relatively low and decreased slightly from 0.14% to 0.11% for the lower to the wider bandgap materials, respectively. The corresponding $QFLS_{PLQY}$ values are only marginally higher (50–100 meV) compared to the qV_{oc} measured in full devices, where the perovskite is sandwiched between transport layers and contacts. This suggests that the non-radiative losses (difference between $QFLS_{RAD}$ and $QFLS_{PLQY}$) are associated with recombination in the bulk of the perovskite film, and only to a less extent with surface/interface recombination. A similar behavior was previously observed for other vacuum deposited wide bandgap perovskites.[52]

We further tested the properties of the wide bandgap perovskite solar cells upon storing them in an inert atmosphere at 85 °C and periodically measured their *J–V* characteristics (corresponding parameters in **Figure 4**). This protocol is similar to the ISOS protocols reported elsewhere,[73] although it is carried out in inert atmosphere and not in (humid) air as suggested in the ISOS-D-2 and ISOS-D-3 test protocols. This is because testing stability in air is actually much more related to testing the encapsulation of the device, and not the semiconducting materials of the solar cell. As our focus is on the material science, we believe that only working in inert atmosphere can give valuable information.

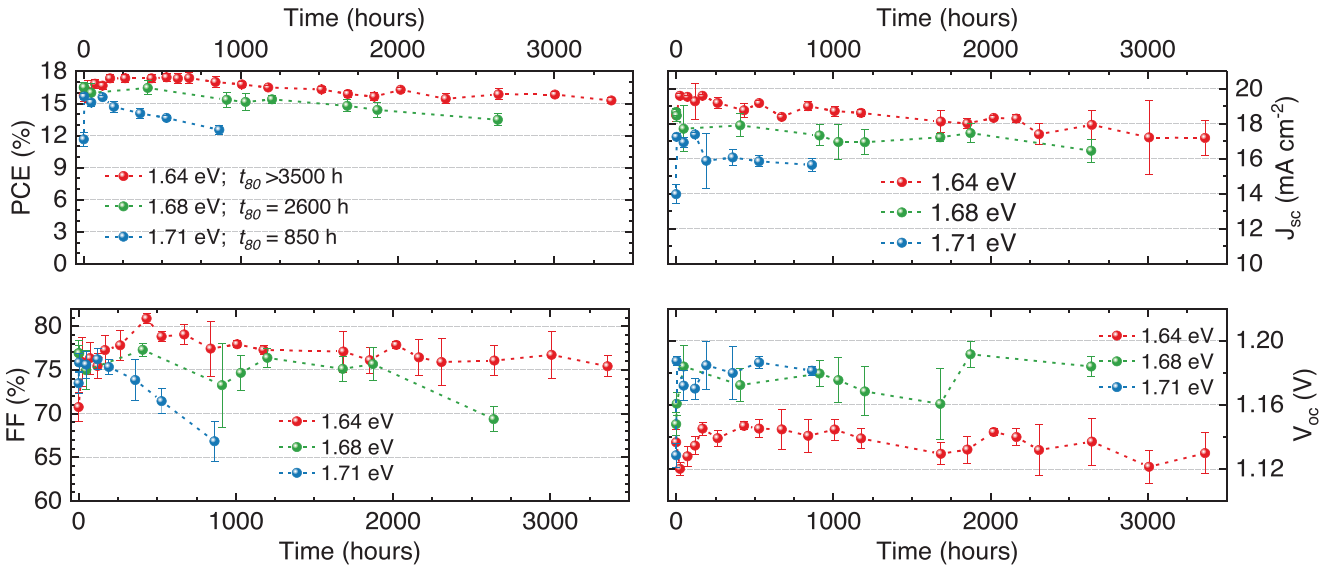

Figure 4. PV parameters extracted from *J–V* curves taken at different times for solar cells kept at 85 °C on a hot plate in a nitrogen filled glovebox.

In general, all the $MAPb(I_{1-x}Br_x)_3$ solar cells were found to be more thermally stable than other previously reported vacuum-deposited wide bandgap devices,[53] and comparable to $MAPbI_3$ solar cells.[55,56] The time to reach 80% of the initial efficiency (t_{80}) was found to exceed 3500 h for the 1.64 eV solar cells and to diminish for perovskite cells with wider bandgap. The 1.68 eV showed a t_{80} of ≈2600 h (which is still remarkable), while the wider bandgap cells (1.71 eV) had a t_{80} of ≈850 h. The main drivers for the device degradation are the current density, monotonically diminishing during thermal stress, and the FF, which was found to decrease faster for wider bandgap devices. The V_{oc}, on the other hand, was found to be rather stable during the thermal stress test. The FF reduction might be also related to the thermal degradation of the organic transport layers, and/or loss of ohmic contact at the electrode interface. In general, however, perovskite formulations with increasing bromide content becomes less thermally stable, as clearly demonstrated recently by high-throughput screening experiments.[74] We also performed measurements under continuous illumination, tracking the maximum power point of a solar cell with bandgap of 1.68 eV (Figure S9, Supporting Information). This initial assessment of light soaking stability suggests that the devices are also stable under continuous illumination, as only a minor decrease of the power output is observed after 6 days.

We prepared ST solar cells with the perovskite with 1.64 eV bandgap, obtained by replacing the Ag top contact with ITO, deposited by pulsed laser deposition (ITO_{PLD}), as recently reported.[75] LiF (100 nm) was used as the anti-reflecting coating (ARC). We chose the most efficient formulation (1.64 eV), and optimized its thickness to maximize the power output of the ST solar cells. We found that the J_{sc} of as-prepared cells can be increased up to >19 mA cm^{-2}, on average (Figure S10a, Supporting Information), by increasing the perovskite thickness to 800 nm. However, the V_{oc} was found to scale inversely with thickness (Figure S10b, Supporting Information), indicating again that non-radiative recombination in the bulk of the perovskite is the main voltage loss for this material. The best trade-off was found for solar cells with the 1.64 eV absorber with 700 nm thick films, leading to a PCE for as-prepared ST solar cells of 15%, on average (Figure S10d, Supporting Information). With the same bandgap and thickness, we also prepared a reference opaque cell with an Ag electrode, which showed a record efficiency of 19.4% after 24 h thermal stress at 85 °C (Figure S11, Supporting Information). As a proof-of-concept, we tested the potential of these $MAPb(I_{1-x}Br_x)_3$ perovskite solar cells in 4T-tandem devices in combination with a mainstream passivated emitter rear cell (PERC) crystalline Si (c-Si) device. For these cells, the top BCP/ITO_{PLD} transparent electrode was substituted with a more NIR transparent top contact, consisting of a SnO_2 buffer layer (40 nm) prepared by spatial ALD (sALD) and a sputtered ITO contact (180 nm), as previously reported.[76,77] An anti-reflective coating (ARC, MgF_2) was deposited on both sides of the devices (glass: 100 nm; ITO: 160 nm).

Figure 5a shows the *J–V* curves for ST perovskite solar cells completed with sALD and sputtered ITO. The as-prepared devices are already well performing without extra post annealing, due to the thermal budget during the sALD process (100 °C for 20 min). Thanks to the use of MgF_2 ARC, the J_{sc} was found to be 19.6 ± 0.2 mA cm^{-2} in the ST configuration. A FF of 74.3% ± 2% and a slightly lower V_{oc} (as compared to reference opaque cells) of 1.13 ± 0.01 V were measured. The latter is related to the different top contact used for these ST devices. The overall PCE was 16.5 ± 0.5% on average, and >17% for the best pixel, as measured from its stabilized power output (inset of Figure 5a). In order to estimate the efficiency of the perovskite solar cell in the tandem configuration, we measured its EQE and transmittance (Figure 5b). The EQE spectrum shows a maximum of 90% in the 500–600 nm range, with the lower values in the NIR region ascribed to non-optimal perovskite thickness.[78] The EQE minimum in the 400–500 nm range is due to the low transmittance of the commercial glass/ITO substrate used (Figure S12, Supporting Information). The small mismatch between the glass/ITO transmittance and device

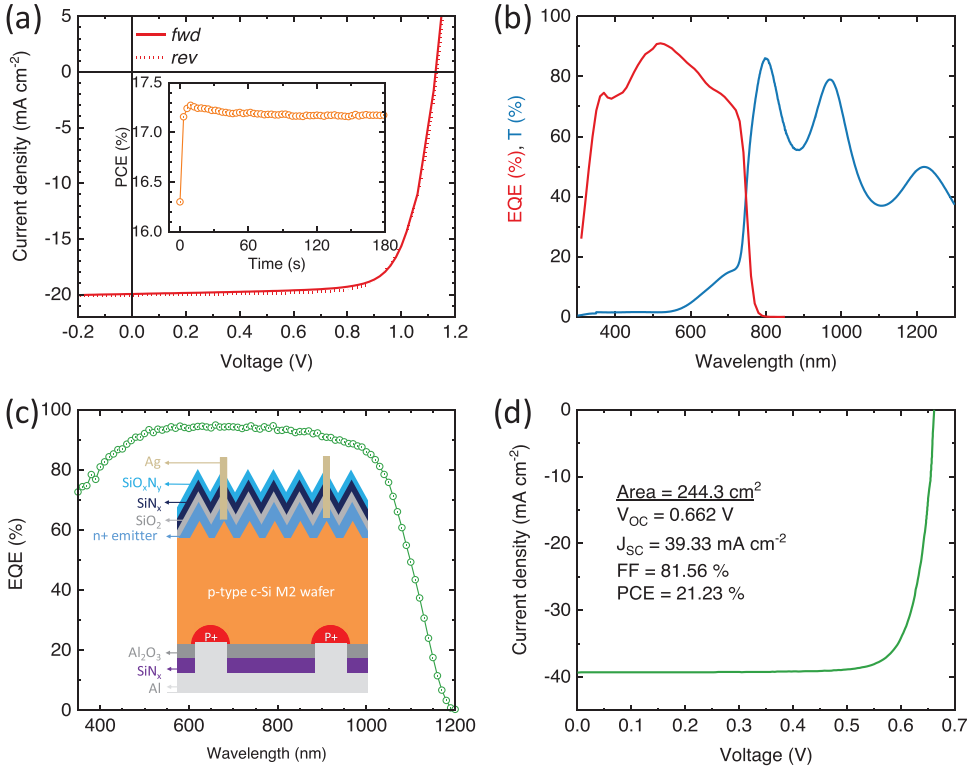

Figure 5. a) *J–V* curves measured under simulated solar illumination for a semitransparent perovskite solar cells with 700 nm thick $MAPb(I_{1-x}Br_x)_3$. Inset shows the stabilized power output for the same device. b) EQE (red) and transmittance spectra (T, blue) of the same device. c) EQE spectrum of a PERC type Si solar cell; in the inset, a schematic of the Si solar cell layout is shown. d) *J–V* curve measured under simulated solar illumination for the same Si solar cell.

EQE spectra might be due to a different reflectance of the two systems. Also the transparency of the full stack was rather low in the NIR, due to the high absorptance of the substrate (Figure S13, Supporting Information) and to unfavorable interference fringes. As a bottom cell, we used a PERC silicon solar cells fabricated on M2 (156.75 × 156.75 mm^2) p-type crystalline silicon (c-Si) wafers (photographs of the semitransparent perovskite cell and of the PERC Si cell are shown in Figure S14,S15, Supporting Information, respectively). Details of the c-Si solar cells fabrication are reported in the supplementary information, and the device layout is illustrated in Figure 5c. The integrated current density estimated from the EQE spectrum of the PERC Si solar cell was 38.2 mA cm^{-2}, and the solar cell delivered a PCE efficiency of 21.23%, as measured by its *J–V* characteristics (Figure 5d, PV parameters are also reported).

Due to the large area mismatch between the ST perovskite cell and the c-Si solar cell, it is not possible to directly measure the two devices in a 4T-tandem configuration. Thus, to estimate its efficiency, we used the optical transmittance of the ST perovskite device, and calculated the filtered efficiency of the bottom c-Si cell, assuming the ST perovskite device is used as a top cell.[76] Details of the method used to calculate the tandem efficiency are reported in the Supporting Information. Due to the low NIR transparency of the glass/ITO substrate of the ST perovskite cell, the current density of the filtered c-Si cell is strongly reduced to 12.7 mA cm^{-2}. Taking into account the rest of the parameters for the filtered bottom c-Si (see **Table 2**), the efficiency of the tandem device is estimated to be 23.3%, a 2.1% absolute gain as compared to the single junction c-Si. The overall 4T-tandem efficiency is limited on one hand by the low NIR transparency of the glass/ITO substrate used for the ST perovskite solar cell fabrication. If the NIR transparency were improved to above 90%, as shown previously by some of us,[76] using a validated calculation for 4T-perovskite/Si tandem cells we estimated the efficiency of our 4T-tandem with PERC Si cell to be 26.5%.[79] On the other hand, the efficiency could be

Table 2. Performance parameters for the ST perovskite solar cell, the c-Si cell, and the 4T-tandem device.

Cell type	Description	V_{oc} [V]	J_{sc} [mA cm^{-2}]	FF [%]	PCE [%]
ST perovskite	Reverse scan	1.14	19.9	74.9	17.0
c-Si	Single junction	0.662	39.3	81.6	21.2
c-Si	Bottom cell	0.629	12.7	78.8	6.3
4T-tandem		–	–	–	23.3

further enhanced by using a more efficient Si solar cell, such as interdigitated back contact (IBC) or heterojunction (HJT) crystalline silicon cells.

3. Conclusion

In summary, we present a simple process to obtain wide bandgap perovskite solar cells via dual-source vacuum deposition. This is possible when a mixed bromide/iodide lead precursor is pre-formed and sublimed as a single component. The bandgap of the perovskite can be simply tuned by changing the bromide content in the precursor compound. The $MAPb(I_{1-x}Br_x)_3$ films have been tested in vacuum deposited solar cells, leading to efficient devices, comparable or even superior to those obtained with mixed cation perovskite formulations. Importantly, the $MAPb(I_{1-x}Br_x)_3$ solar cells are found to be highly thermally stable, with lifetimes (estimated as the time to reach 80% of the initial efficiency) in the order of thousands of hours, depending on the bandgap. This finding agrees with what was previously observed for vacuum deposited $MAPbI_3$, and is somewhat in contrast with reports on solution-processed perovskite cells, where methylammonium is typically used as a minority cation to ensure stability. As a proof-of-concept, we fabricated $MAPb(I_{1-x}Br_x)_3$ solar cells in a semitransparent configuration obtaining stabilized power efficiency exceeding 17%, and estimated their power output in 4T-tandem devices with a mainstream PERC silicon bottom cell. Future studies will be directed towards the development of 2T-tandem devices, either with silicon or with other complementary absorbers.

4. Experimental Section

A detailed description of the materials and methods is available in the Supporting Information.

Supporting Information

Supporting Information is available from the Wiley Online Library or from the author.

Acknowledgements

The authors acknowledge funding through the project "HIPER XL", supported under the umbrella of SOLAR-ERA.NET Cofund by RVO (NL, 1921202), Tubitak (TR, 120N519), AEI (ES, PCI2020-112084). SOLAR-ERA.NET is supported by the European Commission within the EU Framework Programme for Research and Innovation HORIZON 2020 (Cofund ERA-NET Action, N° 691664). The research leading to these results has received funding from the European Research Council (ERC) under the European Union's Horizon 2020 research and innovation programme (Grant agreement No. 834431). This project has received funding from the European Union's Horizon 2020 research and innovation programme under grant agreement N°100862055 (Project NanoQI). Authors acknowledge support from the Comunitat Valenciana: H.B. for projects IDIFEDER/2018/061 and PROMETEU/2020/077; M.S. for project CISEJI/2022/43. Authors acknowledge also support by the Ministry of Science and Innovation (MCIN), and the Spanish State Research Agency (AEI): project PCI2020-112084 funded by MCIN/AEI/10.13039/501100011033 and by the "European Union NextGenerationEU/PRTR"; project CEX2019-000919-M funded by MCIN/AEI/10.13039/501100011033; L.G.E. for grant IJC2019-039851-I funded by MCIN/AEI/10.13039/501100011033; M.S. for grant RYC-2016-21316 funded by MCIN/AEI/10.13039/501100011033 and by "ESF Investing in your future".

Conflict of Interest

The authors declare no conflict of interest.

Data Availability Statement

The data that support the findings of this study are available from the corresponding author upon reasonable request.

Keywords

perovskite solar cells, semi transparent perovskites, vacuum deposition, thermal stability, 4T-tandem

Received: December 8, 2022
Revised: March 23, 2023
Published online: April 25, 2023

[1] J. Jeong, M. Kim, J. Seo, H. Lu, P. Ahlawat, A. Mishra, Y. Yang, M. A. Hope, F. T. Eickemeyer, M. Kim, Y. J. Yoon, I. W. Choi, B. P. Darwich, S. J. Choi, Y. Jo, J. H. Lee, B. Walker, S. M. Zakeeruddin, L. Emsley, U. Rothlisberger, A. Hagfeldt, D. S. Kim, M. Grätzel, J. Y. Kim, *Nature* **2021**, *592*, 381.

[2] H. Min, D. Y. Lee, J. Kim, G. Kim, K. S. Lee, J. Kim, M. J. Paik, Y. K. Kim, K. S. Kim, M. G. Kim, T. J. Shin, S. Il Seok, *Nature* **2021**, *598*, 444.

[3] F. Hao, C. C. Stoumpos, R. P. H. Chang, M. G. Kanatzidis, *J. Am. Chem. Soc.* **2014**, *136*, 8094.

[4] A. Rajagopal, R. J. Stoddard, H. W. Hillhouse, A. K.-Y. Jen, *J. Mater. Chem. A* **2019**, *7*, 16285.

[5] J. H. Noh, S. H. Im, J. H. Heo, T. N. Mandal, S. Il Seok, *Nano Lett.* **2013**, *13*, 1764.

[6] L. Protesescu, S. Yakunin, M. I. Bodnarchuk, F. Krieg, R. Caputo, C. H. Hendon, R. X. Yang, A. Walsh, M. V. Kovalenko, *Nano Lett.* **2015**, *15*, 3692.

[7] M. Jošt, L. Kegelmann, L. Korte, S. Albrecht, *Adv. Energy Mater.* **2020**, *10*, 1904102.

[8] G. E. Eperon, T. Leijtens, K. A. Bush, R. Prasanna, T. Green, J. T.-W. Wang, D. P. McMeekin, G. Volonakis, R. L. Milot, R. May, A. Palmstrom, D. J. Slotcavage, R. A. Belisle, J. B. Patel, E. S. Parrott, R. J. Sutton, W. Ma, F. Moghadam, B. Conings, A. Babayigit, H.-G. Boyen, S. Bent, F. Giustino, L. M. Herz, M. B. Johnston, M. D. McGehee, H. J. Snaith, *Science (80-.)*. **2016**, *354*, 861.

[9] D. Zhao, Y. Yu, C. Wang, W. Liao, N. Shrestha, C. R. Grice, A. J. Cimaroli, L. Guan, R. J. Ellingson, K. Zhu, X. Zhao, R.-G. Xiong, Y. Yan, *Nat. Energy* **2017**, *2*, 17018.

[10] J. Tong, Z. Song, D. H. Kim, X. Chen, C. Chen, A. F. Palmstrom, P. F. Ndione, M. O. Reese, S. P. Dunfield, O. G. Reid, J. Liu, F. Zhang, S. P. Harvey, Z. Li, S. T. Christensen, G. Teeter, D. Zhao, M. M. Al-Jassim, M. F. A. M. van Hest, M. C. Beard, S. E. Shaheen, J. J. Berry, Y. Yan, K. Zhu, *Science (80-.)*. **2019**, *364*, 475.

[11] R. Lin, K. Xiao, Z. Qin, Q. Han, C. Zhang, M. Wei, M. I. Saidaminov, Y. Gao, J. Xu, M. Xiao, A. Li, J. Zhu, E. H. Sargent, H. Tan, *Nat. Energy* **2019**, *4*, 864.
[12] J. Tong, Q. Jiang, A. J. Ferguson, A. F. Palmstrom, X. Wang, J. Hao, S. P. Dunfield, A. E. Louks, S. P. Harvey, C. Li, H. Lu, R. M. France, S. A. Johnson, F. Zhang, M. Yang, J. F. Geisz, M. D. McGehee, M. C. Beard, Y. Yan, D. Kuciauskas, J. J. Berry, K. Zhu, *Nat. Energy* **2022**, *7*, 642.
[13] B. Abdollahi Nejand, D. B. Ritzer, H. Hu, F. Schackmar, S. Moghadamzadeh, T. Feeney, R. Singh, F. Laufer, R. Schmager, R. Azmi, M. Kaiser, T. Abzieher, S. Gharibzadeh, E. Ahlswede, U. Lemmer, B. S. Richards, U. W. Paetzold, *Nat. Energy* **2022**, *7*, 620.
[14] C. Wang, Y. Zhao, T. Ma, Y. An, R. He, J. Zhu, C. Chen, S. Ren, F. Fu, D. Zhao, X. Li, *Nat. Energy* **2022**, *7*, 744.
[15] Q. Han, Y.-T. Hsieh, L. Meng, J.-L. Wu, P. Sun, E.-P. Yao, S.-Y. Chang, S.-H. Bae, T. Kato, V. Bermudez, Y. Yang, *Science (80-.)* **2018**, *361*, 904.
[16] M. Jošt, E. Köhnen, A. Al-Ashouri, T. Bertram, Š. Tomšič, A. Magomedov, E. Kasparavicius, T. Kodalle, B. Lipovšek, V. Getautis, R. Schlatmann, C. A. Kaufmann, S. Albrecht, M. Topič, *ACS Energy Lett.* **2022**, *7*, 1298.
[17] K. O. Brinkmann, T. Becker, F. Zimmermann, C. Kreusel, T. Gahlmann, M. Theisen, T. Haeger, S. Olthof, C. Tückmantel, M. Günster, T. Maschwitz, F. Göbelsmann, C. Koch, D. Hertel, P. Caprioglio, F. Peña-Camargo, L. Perdigón-Toro, A. Al-Ashouri, L. Merten, A. Hinderhofer, L. Gomell, S. Zhang, F. Schreiber, S. Albrecht, K. Meerholz, D. Neher, M. Stolterfoht, T. Riedl, *Nature* **2022**, *604*, 280.
[18] P. Löper, S.-J. Moon, S. Martín de Nicolas, B. Niesen, M. Ledinsky, S. Nicolay, J. Bailat, J.-H. Yum, S. De Wolf, C. Ballif, *Phys. Chem. Chem. Phys.* **2015**, *17*, 1619.
[19] B. Chen, Y. Bai, Z. Yu, T. Li, X. Zheng, Q. Dong, L. Shen, M. Boccard, A. Gruverman, Z. Holman, J. Huang, *Adv. Energy Mater.* **2016**, *6*, 1601128.
[20] G. Coletti, S. L. Luxembourg, L. J. Geerligs, V. Rosca, A. R. Burgers, Y. Wu, L. Okel, M. Kloos, F. J. K. Danzl, M. Najafi, D. Zhang, I. Dogan, V. Zardetto, F. Di Giacomo, J. Kroon, T. Aernouts, J. Hüpkes, C. H. Burgess, M. Creatore, R. Andriessen, S. Veenstra, *ACS Energy Lett.* **2020**, *5*, 1676.
[21] S. Gharibzadeh, I. M. Hossain, P. Fassl, B. A. Nejand, T. Abzieher, M. Schultes, E. Ahlswede, P. Jackson, M. Powalla, S. Schäfer, M. Rienäcker, T. Wietler, R. Peibst, U. Lemmer, B. S. Richards, U. W. Paetzold, *Adv. Funct. Mater.* **2020**, *30*, 1909919.
[22] Z. Wang, X. Zhu, S. Zuo, M. Chen, C. Zhang, C. Wang, X. Ren, Z. Yang, Z. Liu, X. Xu, Q. Chang, S. Yang, F. Meng, Z. Liu, N. Yuan, J. Ding, S. (Frank) Liu, D. Yang, *Adv. Funct. Mater.* **2020**, *30*, 1908298.
[23] E. Lamanna, F. Matteocci, E. Calabrò, L. Serenelli, E. Salza, L. Martini, F. Menchini, M. Izzi, A. Agresti, S. Pescetelli, S. Bellani, A. E. Del Río, Castillo, F. , Bonaccorso, M. , Tucci, A. , DiC. , *Joule* **2020**, *4*, 865.
[24] D. Yang, X. Zhang, Y. Hou, K. Wang, T. Ye, J. Yoon, C. Wu, M. Sanghadasa, S. (Frank) Liu, S. Priya, *Nano Energy* **2021**, *84*, 105934.
[25] K. A. Bush, A. F. Palmstrom, Z. J. Yu, M. Boccard, R. Cheacharoen, J. P. Mailoa, D. P. McMeekin, R. L. Z. Hoye, C. D. Bailie, T. Leijtens, I. M. Peters, M. C. Minichetti, N. Rolston, R. Prasanna, S. Sofia, D. Harwood, W. Ma, F. Moghadam, H. J. Snaith, T. Buonassisi, Z. C. Holman, S. F. Bent, M. D. McGehee, *Nat. Energy* **2017**, *2*, 17009.
[26] F. Sahli, J. Werner, B. A. Kamino, M. Bräuninger, R. Monnard, B. Paviet-Salomon, L. Barraud, L. Ding, J. J. Diaz Leon, D. Sacchetto, G. Cattaneo, M. Despeisse, M. Boccard, S. Nicolay, Q. Jeangros, B. Niesen, C. Ballif, *Nat. Mater.* **2018**, *17*, 820.
[27] J. Xu, C. C. Boyd, Z. J. Yu, A. F. Palmstrom, D. J. Witter, B. W. Larson, R. M. France, J. Werner, S. P. Harvey, E. J. Wolf, W. Weigand, S. Manzoor, M. F. A. M. van Hest, J. J. Berry, J. M. Luther, Z. C. Holman, M. D. McGehee, *Science* **2020**, *367*, 1097.
[28] A. Al-Ashouri, E. Köhnen, B. Li, A. Magomedov, H. Hempel, P. Caprioglio, J. A. Márquez, A. B. Morales Vilches, E. Kasparavicius, J. A. Smith, N. Phung, D. Menzel, M. Grischek, L. Kegelmann, D. Skroblin, C. Gollwitzer, T. Malinauskas, M. Jošt, G. Matič, B. Rech, R. Schlatmann, M. Topič, L. Korte, A. Abate, B. Stannowski, D. Neher, M. Stolterfoht, T. Unold, V. Getautis, S. Albrecht, *Science* **2020**, *370*, 1300.
[29] Y. Hou, E. Aydin, M. De Bastiani, C. Xiao, F. H. Isikgor, D.-J. Xue, B. Chen, H. Chen, B. Bahrami, A. H. Chowdhury, A. Johnston, S.-W. Baek, Z. Huang, M. Wei, Y. Dong, J. Troughton, R. Jalmood, A. J. Mirabelli, T. G. Allen, E. Van Kerschaver, M. I. Saidaminov, D. Baran, Q. Qiao, K. Zhu, S. De Wolf, E. H. Sargent, *Science* **2020**, *367*, 1135.
[30] J. Liu, M. De Bastiani, E. Aydin, G. T. Harrison, Y. Gao, R. R. Pradhan, M. K. Eswaran, M. Mandal, W. Yan, A. Seitkhan, M. Babics, A. S. Subbiah, E. Ugur, F. Xu, L. Xu, M. Wang, A. ur Rehman, A. Razzaq, J. Kang, R. Azmi, A. A. Said, F. H. Isikgor, T. G. Allen, D. Andrienko, U. Schwingenschlögl, F. Laquai, S. De Wolf, *Science* **2022**, *377*, 302.
[31] T. Leijtens, K. A. Bush, R. Prasanna, M. D. McGehee, *Nat. Energy* **2018**, *3*, 828.
[32] E. T. Hoke, D. J. Slotcavage, E. R. Dohner, A. R. Bowring, H. I. Karunadasa, M. D. McGehee, *Chem. Sci.* **2015**, *6*, 613.
[33] D. P. McMeekin, G. Sadoughi, W. Rehman, G. E. Eperon, M. Saliba, M. T. Horantner, A. Haghighirad, N. Sakai, L. Korte, B. Rech, M. B. Johnston, L. M. Herz, H. J. Snaith, *Science* **2016**, *351*, 151.
[34] K. A. Bush, K. Frohna, R. Prasanna, R. E. Beal, T. Leijtens, S. A. Swifter, M. D. McGehee, *ACS Energy Lett.* **2018**, *3*, 428.
[35] S. Gharibzadeh, B. Abdollahi Nejand, M. Jakoby, T. Abzieher, D. Hauschild, S. Moghadamzadeh, J. A. Schwenzer, P. Brenner, R. Schmager, A. A. Haghighirad, L. Weinhardt, U. Lemmer, B. S. Richards, I. A. Howard, U. W. Paetzold, *Adv. Energy Mater.* **2019**, *9*, 1803699.
[36] A. Rajagopal, R. J. Stoddard, S. B. Jo, H. W. Hillhouse, A. K. Y. Jen, *Nano Lett.* **2018**, *18*, 3985.
[37] F. Peña-Camargo, P. Caprioglio, F. Zu, E. Gutierrez-Partida, C. M. Wolff, K. Brinkmann, S. Albrecht, T. Riedl, N. Koch, D. Neher, M. Stolterfoht, *ACS Energy Lett.* **2020**, *5*, 2728.
[38] H. Xie, M. Lira-Cantu, *J. Phys. Energy* **2020**, *2*, 024008.
[39] D. P. McMeekin, G. Sadoughi, W. Rehman, G. E. Eperon, M. Saliba, M. T. Hörantner, A. Haghighirad, N. Sakai, L. Korte, B. Rech, M. B. Johnston, L. M. Herz, H. J. Snaith, *Science* **2016**, *351*, 151.
[40] D. J. Slotcavage, H. I. Karunadasa, M. D. McGehee, *ACS Energy Lett.* **2016**, *1*, 1199.
[41] J. Li, H. Wang, X. Y. Chin, H. A. Dewi, K. Vergeer, T. W. Goh, J. W. M. Lim, J. H. Lew, K. P. Loh, C. Soci, T. C. Sum, H. J. Bolink, N. Mathews, S. Mhaisalkar, A. Bruno, *Joule* **2020**, *4*, 1035.
[42] J. Feng, Y. Jiao, H. Wang, X. Zhu, Y. Sun, M. Du, Y. Cao, D. Yang, S. (Frank) Liu, *Energy Environ. Sci.* **2021**, *14*, 3035.
[43] C. Momblona, O. Malinkiewicz, C. Roldán-Carmona, A. Soriano, L. Gil-Escrig, E. Bandiello, M. Scheepers, E. Edri, H. J. Bolink, *APL Mater.* **2014**, *2*, 081504.
[44] J. B. Patel, A. D. Wright, K. B. Lohmann, K. Peng, C. Q. Xia, J. M. Ball, N. K. Noel, T. W. Crothers, J. Wong-Leung, H. J. Snaith, L. M. Herz, M. B. Johnston, *Adv. Energy Mater.* **2020**, *10*, 1903653.
[45] D. Forgács, L. Gil-Escrig, D. Pérez-Del-Rey, C. Momblona, J. Werner, B. Niesen, C. Ballif, M. Sessolo, H. J. Bolink, *Adv. Energy Mater.* **2017**, *7*, 1602121.
[46] C. Momblona, L. Gil-Escrig, E. Bandiello, E. M. Hutter, M. Sessolo, K. Lederer, J. Blochwitz-Nimoth, H. J. Bolink, *Energy Environ. Sci.* **2016**, *9*, 3456.

[47] M. Roß, L. Gil-Escrig, A. Al-Ashouri, P. Tockhorn, M. Jošt, B. Rech, S. Albrecht, *ACS Appl. Mater. Interfaces* **2020**, *12*, 39261.
[48] K. B. Lohmann, S. G. Motti, R. D. J. Oliver, A. J. Ramadan, H. C. Sansom, Q. Yuan, K. A. Elmestekawy, J. B. Patel, J. M. Ball, L. M. Herz, H. J. Snaith, M. B. Johnston, *ACS Energy Lett.* **2022**, *7*, 1903.
[49] H. Li, J. Zhou, L. Tan, M. Li, C. Jiang, S. Wang, X. Zhao, Y. Liu, Y. Zhang, Y. Ye, W. Tress, C. Yi, *Sci. Adv.* **2022**, *8*, eabo7422.
[50] L. Gil-Escrig, C. Momblona, M.-G. La-Placa, P. P. Boix, M. Sessolo, H. J. Bolink, *Adv. Energy Mater.* **2018**, *8*, 1703506.
[51] R. Ji, Z. Zhang, C. Cho, Q. An, F. Paulus, M. Kroll, M. Löffler, F. Nehm, B. Rellinghaus, K. Leo, Y. Vaynzof, *J. Mater. Chem. C* **2020**, *8*, 7725.
[52] L. Gil-Escrig, C. Dreessen, F. Palazon, Z. Hawash, E. Moons, S. Albrecht, M. Sessolo, H. J. Bolink, *ACS Energy Lett.* **2021**, *6*, 827.
[53] I. Susic, L. Gil-Escrig, F. Palazon, M. Sessolo, H. J. Bolink, *ACS Energy Lett.* **2022**, *7*, 1355.
[54] B. Conings, J. Drijkoningen, N. Gauquelin, A. Babayigit, J. D'Haen, L. D'Olieslaeger, A. Ethirajan, J. Verbeeck, J. Manca, E. Mosconi, F. De Angelis, H.-G. Boyen, *Adv. Energy Mater.* **2015**, *5*, 1500477.
[55] H. A. Dewi, J. Li, H. Wang, B. Chaudhary, N. Mathews, S. Mhaisalkar, A. Bruno, *Adv. Funct. Mater.* **2021**, *31*, 2100557.
[56] I. C. Kaya, K. P. S. Zanoni, F. Palazon, M. Sessolo, H. Akyildiz, S. Sonmezoglu, H. J. Bolink, *Adv. Energy Sustain. Res.* **2021**, *2*, 2000065.
[57] G. Longo, C. Momblona, M.-G. La-Placa, L. Gil-Escrig, M. Sessolo, H. J. Bolink, *ACS Energy Lett.* **2018**, *3*, 214.
[58] J. Huang, S. Xiang, J. Yu, C.-Z. Li, *Energy Environ. Sci.* **2019**, *12*, 929.
[59] H. A. Dewi, J. Li, E. Erdenebileg, H. Wang, M. De Bastiani, S. De Wolf, N. Mathews, S. Mhaisalkar, A. Bruno, *Sustain. Energy Fuels* **2022**, *6*, 2428.
[60] A. M. Igual-Muñoz, J. Navarro-Alapont, C. Dreessen, F. Palazon, M. Sessolo, H. J. Bolink, *Chem. Mater.* **2020**, *32*, 8641.
[61] H. Li, L. Tan, C. Jiang, M. Li, J. Zhou, Y. Ye, Y. Liu, C. Yi, *Adv. Funct. Mater.* **2023**, *33*, 2211232.
[62] C.-W. Chen, H.-W. Kang, S.-Y. Hsiao, P.-F. Yang, K.-M. Chiang, H.-W. Lin, *Adv. Mater.* **2014**, *26*, 6647.
[63] S.-Y. Hsiao, H.-L. Lin, W.-H. Lee, W.-L. Tsai, K.-M. Chiang, W.-Y. Liao, C.-Z. Ren-Wu, C.-Y. Chen, H.-W. Lin, *Adv. Mater.* **2016**, *28*, 7013.
[64] B.-S. Kim, L. Gil-Escrig, M. Sessolo, H. J. Bolink, *J. Phys. Chem. Lett.* **2020**, *11*, 6852.
[65] K. P. S. Zanoni, L. Martínez-Goyeneche, C. Dreessen, M. Sessolo, H. J. Bolink, *Sol. RRL* **2023**, *7*, 2201073.
[66] K. B. Lohmann, J. B. Patel, M. U. Rothmann, C. Q. Xia, R. D. J. Oliver, L. M. Herz, H. J. Snaith, M. B. Johnston, *ACS Energy Lett.* **2020**, *5*, 710.
[67] T. Abzieher, T. Feeney, F. Schackmar, Y. J. Donie, I. M. Hossain, J. A. Schwenzer, T. Hellmann, T. Mayer, M. Powalla, U. W. Paetzold, *Adv. Funct. Mater.* **2021**, *31*, 2104482.
[68] I. Susic, K. P. S. Zanoni, A. Paliwal, I. C. Kaya, Z. Hawash, M. Sessolo, E. Moons, H. J. Bolink, *Sol. RRL* **2022**, *6*, 2100882.
[69] E. Smecca, V. Valenzano, S. Valastro, I. Deretzis, G. Mannino, G. Malandrino, G. Accorsi, S. Colella, A. Rizzo, A. La Magna, A. Listorti, A. Alberti, *J. Mater. Chem. A* **2021**, *9*, 16456.
[70] U. Rau, *Phys. Rev. B* **2007**, *76*, 085303.
[71] S. Rühle, *Sol. Energy* **2016**, *130*, 139.
[72] T. P. A. van der Pol, K. Datta, M. M. Wienk, R. A. J. Janssen, *Adv. Opt. Mater.* **2022**, *10*, 2102557.
[73] M. V. Khenkin, E. A. Katz, A. Abate, G. Bardizza, J. J. Berry, C. Brabec, F. Brunetti, V. Bulović, Q. Burlingame, A. Di Carlo, R. Cheacharoen, Y.-B. Cheng, A. Colsmann, S. Cros, K. Domanski, M. Dusza, C. J. Fell, S. R. Forrest, Y. Galagan, D. Di Girolamo, M. Grätzel, A. Hagfeldt, E. von Hauff, H. Hoppe, J. Kettle, H. Köbler, M. S. Leite, S. Liu, Y.-L. Loo, J. M. Luther, et al., *Nat. Energy* **2020**, *5*, 35.
[74] Y. Zhao, T. Heumueller, J. Zhang, J. Luo, O. Kasian, S. Langner, C. Kupfer, B. Liu, Y. Zhong, J. Elia, A. Osvet, J. Wu, C. Liu, Z. Wan, C. Jia, N. Li, J. Hauch, C. J. Brabec, *Nat. Energy* **2021**, *7*, 144.
[75] K. P. S. Zanoni, A. Paliwal, M. A. Hernández-Fenollosa, P. Repecaud, M. Morales-Masis, H. J. Bolink, *Adv. Mater. Technol.* **2022**, *7*, 2101747.
[76] D. Zhang, M. Najafi, V. Zardetto, M. Dörenkämper, X. Zhou, S. Veenstra, L. J. Geerligs, T. Aernouts, R. Andriessen, *Sol. Energy Mater. Sol. Cells* **2018**, *188*, 1.
[77] J. Wang, V. Zardetto, K. Datta, D. Zhang, M. M. Wienk, R. A. J. Janssen, *Nat. Commun.* **2020**, *11*, 5254.
[78] M. Koç, W. Soltanpoor, G. Bektaş, H. J. Bolink, S. Yerci, *Adv. Opt. Mater.* **2019**, *7*, 1900944.
[79] D. Zhang, K. Datta, V. Zardetto, S. Veenstra, G. Coletti, R. A. J. Janssen, *Sol. RRL* **2022**, *7*, 2200914.